Ultrasmall Nickel Nanoparticles on a Covalent Triazine Framework for Ammonia Borane Hydrolysis and Transfer Hydrogenation of Nitroaromatics

Esther Punzi[a], *Xuan Trung Nguyen*[a], *Emanuela Pitzalis*[a], *Alessandro Mandoli*[b], *Massimo Onor*[a], *Marcello Marelli*[c], *Lorenzo Poggini,*[d,e] *Giulia Tuci*[d] *Giuliano Giambastiani*[d,e]*, *Claudio Evangelisti*[a]*

[a] CNR-ICCOM, Institute of Chemistry of Organo Metallic Compounds, Via G. Moruzzi 1, 56124 Pisa, Italy;

[b] Department of Chemistry and Industrial Chemistry, University of Pisa, Via G. Moruzzi 13, 56124 Pisa, Italy;

[c] CNR-SCITEC, Institute of Science and Chemical Technologies "Giulio Natta", Via Fantoli 16/15, 20138 Milano, Italy;

[d] CNR-ICCOM, Institute of Chemistry of Organo Metallic Compounds, ICCOM-CNR, Via Madonna del Piano 10, Sesto Fiorentino, Italy;

[e]Department of Chemistry "U. Schiff" - DICUS – and INSTM Research Unit, University of Florence, Via della Lastruccia 3-13, 50019 Sesto Fiorentino (FI), Italy

Corresponding Authors: Giuliano Giambastiani (giuliano.giambastiani@iccom.cnr.it); Claudio Evangelisti (claudio.evangelisti@cnr.it)

ABSTRACT

Ammonia borane (AB) is a promising candidate as hydrogen reservoir both in terms of dihydrogen storage and hydrogen source for transfer hydrogenation (TH) to unsaturated organic substrates. Ultrasmall Ni nanoparticles (NPs) have been synthesized by metal vapor synthesis (MVS) and supported on a covalent-triazine framework (CTF^{Ph}). The physical and chemical properties of the Ni/CTF^{Ph} nanocomposite have been thoroughly investigated. Despite the high Ni loading (10 wt.%), the material shows well-dispersed ultrasmall Ni nanoparticles (2.2 nm), unveiling the non-innocent role of N-doped templating carrier towards NPs dispersion and stabilization. The Ni/CTF^{Ph} has shown excellent catalytic performance in the AB hydrolysis and AB transfer hydrogenation (AB-TH) for the conversion of a variety of nitroarenes, including halogen-substituted ones, into the corresponding anilines. As for the latter process, Ni/CTF^{Ph} has unveiled a remarkable catalytic efficiency, durability and reusability under both batch and continuous flow operative conditions. Noteworthily, whatever the catalytic process at work, Ni/CTF^{Ph} certainly ranks or even outperforms most Ni-based systems of the *state-of-the-art*, including its Ni/VXC analogue (Ni 10 wt.% prepared by MVS technique) synthesized from a plain and undoped carbon support (*i.e.*, Vulcan XC-72R).

KEYWORDS: Hydrogen generation, Ammonia Borane, Hydrogenation, Ni catalyst, Covalent Triazine Framework, Heterogeneous catalysis.

1. INTRODUCTION

Ammonia borane (AB, H_3N-BH_3) is a cheap inorganic salt that has emerged as an effective hydrogen storage material due to its high gravimetric hydrogen storage capacity (up to 19.6 wt.%).[1] This feature, along with its easy preparation (*i.e.*, from sodium borohydride and ammonium carbonate), non-toxicity and stability, have made it a key component of the chemical hydrogen storage technology for the on-demand and sustainable supply of dihydrogen as energy vector.[2] The chemically stored hydrogen can be released by the use of a catalyst to kinetically favor H_2 evolution under mild experimental conditions and produces 3 moles of H_2 per AB mole (Equation 1).

$$H_3N - BH_3 + 2H_2O \rightarrow 3H_2 \uparrow + NH_4BO_2 \quad (1)$$

AB is also the reducing agent for a wide range of applications, spanning from the reductive transformation of unsaturated organic compounds to biomass refinement, and fuel production up to the synthesis of pharmacologically active compounds and commodities.[3] Most of these reduction processes make use of pressurized molecular hydrogen gas for the direct substrates hydrogenation (DH) or liquid hydrogen sources such as alcohols,[4] formic acid,[5] and hydrosilanes[6] for transfer hydrogenation (TH) processes. Conventionally, reactions carried out with molecular dihydrogen gas (DH) require specialized equipment for the pressurized and flammable gas manipulation that poses safety concerns. In contrast, TH based on the use of liquid hydrogen sources provides a safer alternative to the process. However, technical concerns such as the often high reaction temperature of alcohols or the equipment corrosion caused by the use of formic acid, have made questionable a practical upscale of this catalytic technology.[3] More recently, AB has emerged as a viable, safer and scalable alternative compared to gaseous and liquid reagents for the catalytic AB hydrolysis and TH reaction.[7] Heterogeneous catalysts from the platinum-group

metals (*e.g.,* Pt, Pd, Ru) rank among the most active systems for AB hydrolysis and TH reactions.[8-13] Anyhow, the search for cheaper, effective and more sustainable catalytic solutions based on the use of abundant transition metal-based systems (*e.g.,* Fe, Cu, Ni, Co) has emerged as a matter of extensive investigation during the last years, unveiling really promising perspectives.[14-23] Among cheaper transition metals, Ni-based catalysts have pointed out excellent performance both for the AB hydrolytic dehydrogenation and AB transfer hydrogenation (TH).[24-26] Strategies aimed at enhancing the performance of these heterogeneous systems essentially lie on the control of the metal nanoparticles (NPs) size and distribution on a given support. Recent reports have unveiled that replacing pure carbon-based carriers with N-doped carbon supports, holds important benefits at the nanoscale that can translate into improved catalytic performance.[27-30] N-dopants in C-carriers deeply modulate their inherent acid-base properties. While their generally high specific surface area and micro-, meso-porosity offer important steric restrictions to confined metal particles,[31-34] N-atoms generate preferential binding sites for the MNPs growth and stabilization.[27,30] These features impart to NPs greater resistance to agglomeration and leaching phenomena, hence resulting in catalytic materials with improved stability and durability.[35] Covalent Triazine framework (CTF) represents an exciting class of highly porous N-rich organic materials (POP, porous organic polymers), easily obtained from the cyclotrimerization of cyano–aryl building blocks in molten zinc chloride.[32,36,37] Their unique structural properties (*i.e.,* predetermined and periodic structure, low material density, high permanent porosity, high specific surface area, and thermal stability) along with their easy structural and chemical tunability have made them ideal candidates for a number of large-scale applications such as molecular separation and storage,[38,39] energy storage,[40] photocatalysis[41] and heterogeneous catalysis.[36,42] As far as AB hydrolysis and TH reaction are concerned, different research groups have already explored on the use of CTFs as

supports for a metal active phase.[23,43,44] Li *et al.* demonstrated the electron donating effect of a N-rich CTF carrier to surface dispersed Co or Ni NPs with respect to the catalyst kinetics in AB hydrolysis. Their study has unveiled how active transition metal NPs with an optimal electron structure may speed up the hydrolysis of AB.[23] More recently, experimental and *in-silico* studies by Wang *et al.* have verified that CTFs carriers modify the surface electronic structure of Pd nanoclusters giving rise to active and stable metal phases suitable to hydrolyze AB effectively or use it under mild experimental conditions as TH catalyst for a wide range of nitroaromatics.[44] Herein, we describe the synthesis and characterization of a Ni-CTF nanocomposite featured by ultrasmall metal NPs obtained by metal vapor synthesis (MVS). MVS allows to obtain almost monodisperse and nanosized ligand-free transition-metal NPs well fit for their immobilization on suitable macrocarriers.[45-49] As far as the current study is concerned, the CTF material prepared from the cyanotrimerization reaction of 1,3- dicyanobenzene (CTF^{Ph}) was selected as carrier for the ultrasmall Ni NPs to get the Ni/CTF^{Ph}, composite **1**. Carbon black (Vulcan XC-72R) was also employed to prepare the Ni/VXC, composite **2**, as a reference catalytic material with a plain carbonaceous.

The as-prepared supported Ni systems have been explored as catalysts for the AB hydrolysis with H_2 production as well as for the AB-TH of various nitroarenes. The superior performance of Ni/CTF^{Ph} (**1**) on both catalytic processes has been discussed and compared with that of its Ni-based counterpart prepared from a plain and undoped C-network Ni/VXC (**2**) as well as those registered for the most relevant and related Ni-based systems of the *state-of-the-art*. As for the AB-TH process, aromatic amines are key building blocks in a wide range of applications and for the manufacturing of high added-value chemicals.[3]

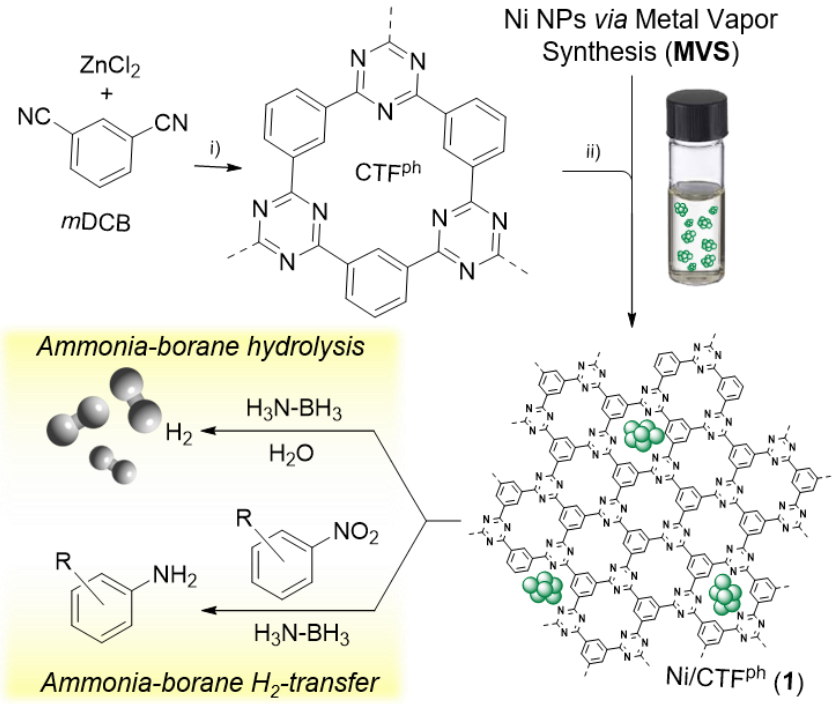

Scheme 1. Synthetic approach to Ni/CTF^{Ph} (**1**) and its catalytic applications in AB hydrolysis and AB-TH of nitroarenes.

A remarkable efficiency, stability and durability of **1** to promote AB-TH of nitroarenes, including halo-substituted ones, has been observed and discussed using batch and continuous flow setups.

2. MATERIALS AND METHODS

All manipulations were carried out using standard Schlenk-type techniques under nitrogen or argon atmosphere. Vulcan XC-72R was provided by Cabot Ltd and used as received. Where not indicated, the reagents and solvents have been used as supplied by the manufacturers. Mesitylene (98%, Merck®) was distilled over metallic Na and then stored in a dry argon atmosphere. All the other products were purchased from Merck® and used without any further purification: borane ammonia complex (purity >95.0%), 1-bromo-4-nitrobenzene (purity >98.0%), 4-nitroaniline

(purity 99.0%), 4-nitrophenol (purity 99.0%), 1-chloro-2-nitrobenzene (purity 99.0%), 1-chloro-4-nitrobenzene (purity 99.0%), nitrobenzene (purity of 99.0%), 4-nitrobenzaldehyde (purity of 98.0%), *n*-pentane (purity 99.0%), ethanol (purity 99.0%). Samples sonication was accomplished with an Elma S15 Elmasonic sonicator bath (37 kHz). UV spectra were acquired with a Jasco V-750 UV-Vis spectrophotometer equipped with integrating sphere. GC-FID (Gas Cromatography-Flame Ionization Detector) chromatograms were recorded with a Shimadzu gas chromatograph GC/FID 2010 PRO, with a capillary column DB-1 (30 m x 0.25 mm inner diameter, 1 μm stationary phase). Gas chromatography coupled to mass spectrometry (GC-MS) was performed with a Gas chromatograph GC/MS equipped with a 5975C MSD (Agilent Technologies) mass detector and a capillary column (DB-5, 30 m x 0.25 mm inner diameter, 0.25 μm stationary phase). N_2-physisorprion measurements were acquired on an ASAP 2020 Micromeritics apparatus after the samples activation at 120 °C for 12 h under high-vacuum. Specific surface area (SSA) was calculated by means of Brunauer-Emmett-Teller (BET) model, while pore size distributions were evaluated by BJH method using the desorption branch of N_2 isotherms. Micropore volumes were estimated by NLDFT approximation method. XPS analyses was carried out in an ultra-high vacuum chamber capable of reaching a pressure lower than 10^{-10} mbar. The radiation used was a non-monochromatized Al (hν = 1486.6 eV, VSW-TA10). The analyzer employed was a hemispherical electron/ion energy analyzer (VSW-HA100 equipped with a 16-channel detector). The X-ray source had an operating power of 120 W (12 kV and 10 mA). The photoelectrons were collected perpendicularly to the surface sample in fixed analyzer transmission mode (pass energy of 44 eV). The XPS spectra calibration was conducted by setting the C sp^2 component of C 1*s* signal to 284.6 eV.[50] The spectra were analyzed using CasaXPS software, and tougaard function was used to subtract the background. The deconvolution of XPS spectra has been performed by applying a combination of Gaussian and Lorentzian functions (70/30 ratio). Transmission Electron Microscopy (TEM)

measurements and related analysis [*i.e.,* imaging, Electron Energy-Loss Spectroscopy (EELS) and electron spectroscopic imaging (ESI)] were performed on a ZEISS libra200FE instrument, equipped with an in-column omega filter analyzer. Specimens were gently ground in an agate mortar, dispersed in 2-propanol, and placed in an ultrasonic bath for 15 minutes to obtain a homogeneous suspension to be drop-casted on a lacey carbon film Cu TEM grid. Samples were analyzed after drying overnight. ICP-OES analyses were carried out with Optima 8000 ICP-OES (Perkin Elmer) operating at 1500W and equipped with autosampler S10, MiraMist® Nebulizer (Perkin Elmer) and cyclonic chamber. Argon (420.069 nm) was used as the internal standard. Ni was examined at 231.604 nm wavelength. 10 mg of material was treated with 3 mL HNO_3 (Fluka, Trace Select for trace analysis >69%) and 1 mL H_2O_2 30% (Sigma Aldrich, >30% for trace analysis) and kept at boiling temperature for three hours, until complete digestion. After cooling, the sample was diluted with ultrapure water containing 2% HNO_3. NMR spectra were recorded with a JEOL YH500 MHz spectrometer, operating at the frequency of 500 MHz for ^{1}H NMR. The ^{1}H NMR resonances are described according to the notation: s (singlet), d (doublet), dd (double doublet), and m (multiplet).

2.1. Synthesis of CTF^{Ph}

CTF^{Ph} was prepared under classical ionothermal conditions following previous literatures procedures.[36,51] In brief, 1,3-dicyanobenzene was mixed with 5 eq. of anhydrous $ZnCl_2$ and transferred in a quartz ampule. After drying under vacuum for 3 h, the ampule was flame-sealed and the sample submitted to a two-steps heating ramp (400 °C for 10 h + 600 °C for 10 h). After cooling to room temperature, the ampule was opened and the recovered solid finely ground and purified by means of sequential washing cycles (water, HCl 1M, NaOH 1M, water and THF). The

sample was finally dried in vacuo to constant weight and stored on air at room temperature. Characterization of the as-prepared material showed results coherent with those reported in the literature.[36]

2.2. Catalyst Synthesis

Ni NPs supported on CTF^{Ph} and on Carbon XC-72R (VXC) were synthesized by the MVS technique (Figure S1) using a previously described lab-scale reactor.[45] Ni vapors, generated at 10^{-5} mbar by resistive heating of an alumina crucible filled with ca. 350 mg of nickel powder, were co-condensed at the liquid nitrogen temperature (-196°C) with mesitylene (100 mL) in the glass reactor chamber of the MVS apparatus. The reactor chamber was heated to the melting point of the solid matrix (ca. - 40°C) and the resulting brown solution siphoned at low temperature in a Schlenk tube and kept in a refrigerator at - 40°C. The nickel content of the obtained Ni-solvated metal atoms was 1.0 mg/mL, as determined by ICP-OES analysis. Accordingly, 5 mL of the solution (5 mg of Ni) was added to a suspension of the selected support (50 mg of CTF^{Ph} or VXC) in mesitylene (5 mL) under dry argon atmosphere. The mixture was stirred for 12 h at room temperature. Afterward, the colorless solution was removed and the obtained solids Ni/CTF^{Ph} (**1**) or Ni/VXC (**2**) were thoroughly washed with *n*-pentane (3 x 10 mL) and dried under reduced pressure (10^{-2} mbar) to constant weight. Both isolated samples contained 10.0 wt.% of Ni as determined by ICP-OES analysis.

2.3. Catalytic AB hydrolysis: general procedure

A 10 mL Schlenk tube was charged under Ar with the Ni catalyst of choice (1.5 mg, Ni 10.0 wt.%, 0.0026 mmol of Ni) and 3 mL of degassed water. The obtained suspension was sonicated

for 2 minutes in an ultrasonic bath, transferred to the reaction cell and maintained under vigorous magnetic stirring (ca. 1000 rpm) at 30°C. Afterwards, the acquisition of the pressure signal started while 200 mL of a 1M AB aqueous solution was injected into the cell (Figure S2). The pressure signal acquisition was maintained throughout the whole experiment and namely until gas evolution was over. The amount of hydrogen evolved was calculated on the basis of the pressure increase in the cell. The catalytic test was repeated three times for each catalyst and their average performance was expressed as Turnover Frequency [TOF = $mol_{H2} \cdot mol_{Ni}^{-1} \cdot min^{-1}$] calculated at an AB conversion of around 33%.

2.4. Catalytic TH of nitroaromatic compounds: general procedure

The proper amount of the selected nitroarene (0.052-0.130 mmol) was placed in a 10 mL Schlenk tube containing the selected Ni catalyst (1.5 mg, Ni 10 wt.%, 0.0026 mmol of Ni) suspended in 3 mL of solvent (H_2O or H_2O/EtOH 10/1 v./v.) The suspension was sonicated for 2 minutes in an ultrasonic bath and then transferred to the reaction cell and maintained under vigorous magnetic stirring (ca. 1000 rpm) until reaching the desired reaction temperature (*i.e.*, 30°C or 45°C). The acquisition of the pressure signal started while 0.25-0.65 mmol of a 1M AB aqueous solution were injected into the cell. The reaction was monitored at constant times by sampling it with a micro syringe (200-250 μL of solution) and analyzing solution contents by UV-vis or GC-FID and GC-MS. The catalysts performance was expressed as Turnover Frequency [TOF = $mol_{sub.\ conv.} \cdot mol_{Ni}^{-1} \cdot min^{-1}$]. The selectivity towards the main product was calculated as $mol_{product} \cdot mol_{sub.\ conv}^{-1}$.

2.5 Recycling tests

The recycling tests on Ni/CTF^{Ph} were carried out in a 50 mL Schlenk tube containing the Ni/CTF^{Ph} (**1**) 10.0 wt. Ni% (6 mg, 0.0104 mmol Ni), suspended in 12 mL of H_2O. The suspension was sonicated for 2 minutes in an ultrasonic bath and maintained under vigorous magnetic stirring (ca. 1000 rpm) until reaching the desired reaction temperature (i.e. 45 °C). Then, 1.0 mmol of a 1M AB aqueous solution were injected tube together with 4-nitrophenol (0.21 mmol). The suspension obtained after the catalytic run was transferred to a 50 mL Falcon Tube and centrifugated as to remove the supernatant from the solid catalyst. The latter was then thoroughly washed with deionized water and suspended in 12 mL of fresh water and used for the further reaction run.

2.6 Catalytic TH of 4-nitrophenol in continuous-flow

The packed-bed continuous-flow reactor (PCFR) was assembled by placing 24.1 mg of Ni/CTF^{ph} (2.4 mg Ni, 0.041 mmol) in an HPLC-like stainless still column (150 cm length × 4.6 mm i.d., nominal internal volume V° = 2.49 cm^3). The column was connected by cuts of PEEK or PTFE tubing (0.5 mm i.d. × 1.5 mm o.d.) at one end to a Uniqsys FlowLab^{TM} system, at the other to a collection Schlenk tube kept under Ar (Figure S12). Before performing the TH run, the catalyst was activated by placing the PCFR in a water bath at 45 °C and flushing for 5 minutes with 0.5 M aqueous AB, delivered through the Channel A of the FlowLab^{TM} device (f_A = 200 µL min^{-1}). Then, the TH run was started by simultaneous pumping the said 0.5 M AB solution (4.2 mmol, f_A = 70 µL min^{-1}) and a 0.017 M aqueous 4-nitrophenol (0.83 mmol, f_B = 407 µL min^{-1}), via the FlowLab^{TM} Channels A and B, respectively, with the streams of the two reactants combined via a static T-mixer placed in the heating bath just before the PCFR inlet. The outcome of the TH reaction was

evaluated by recording the UV-vis spectrum of samples taken at 1 h time interval. A sequence of three consecutive activation-reaction run (2 h each) was carried out, to give the results summarized in Figure S13.

3. RESULT AND DISCUSSION

*3.1. Synthesis and characterization of Ni/CTF^{Ph} (**1**) and Ni/VXC (**2**)*

Ni NPs were synthesized as ligand-free particles in their reduced form by MVS approach[45] and supported on either CTF^{Ph} or VXC to get the composites **1** and **2**, respectively (see Section 2.2). After the deposition, both catalysts were maintained under a dry air atmosphere. ICP-OES analysis of the two catalysts confirmed a quantitative deposition of Ni NPs leading to a final Ni content of 10.0 wt.% on both supports (Table 1). HAADF-STEM and TEM analysis was performed to investigate the structural and morphological features of the as-prepared Ni-catalysts. Ni/CTF^{Ph} (**1**) exhibited NPs homogeneously dispersed on the CTF support (Figure 1, Figure S4) and a narrow particles size distribution (1.0 – 3.5 nm, d_m = 2.2 nm). HR-TEM analysis (Figure 1) shows lattice planes extended to the whole particle without any stacking faults or twins, exhibiting a *d*-spacing of 2.1 Å that are ascribed to the (2 0 0) planes of the cubic structure of NiO. On the other hand, Ni/VXC (**2**) showed NPs sizes slightly larger, ranging mainly from 2 to 4.5 nm (d_m = 2.9 nm), (Figure S3), dispersed onto the support, together with the presence of a small fraction of NPs agglomerates.

In spite of a relatively high Ni loading, the high metal dispersion observed in Ni/CTF^{Ph} is ascribed to the relatively high specific surface area and mesoporous nature of the carbonaceous support as well as to the non-innocent templating action played by N-sites of the doped C-network towards ultra-small Ni NPs obtained by MVS technique. EELS analysis and ESI elemental

mapping (Figure S5) carried out on **1** confirm the presence of N on the whole sample's surface and the oxidized chemical state of Ni NPs, through the typical NiO shift in the spectra.

Figure 2A and 2B refer to the isothermal profiles and pore size distribution measured on **1** and **2**. Table 1, finally details the materials textural properties (Specific surface area (SSA) and pore size distribution). As expected, **1** presented a type IV isotherm with a characteristic H_2 hysteresis loop in the range 0.4–0.6 p/p_0 which is typical of bimodal micro-/mesoporous structures featured by complex pores of ill-defined shape. In particular, it contains micro- and small mesopores mainly centered in the 2 - 8 nm range. On the other hand, **2** presents a type II isotherm with a very moderate hysteresis loop typical of materials with low SSA and micro-, mesopore volumes.[52,53]

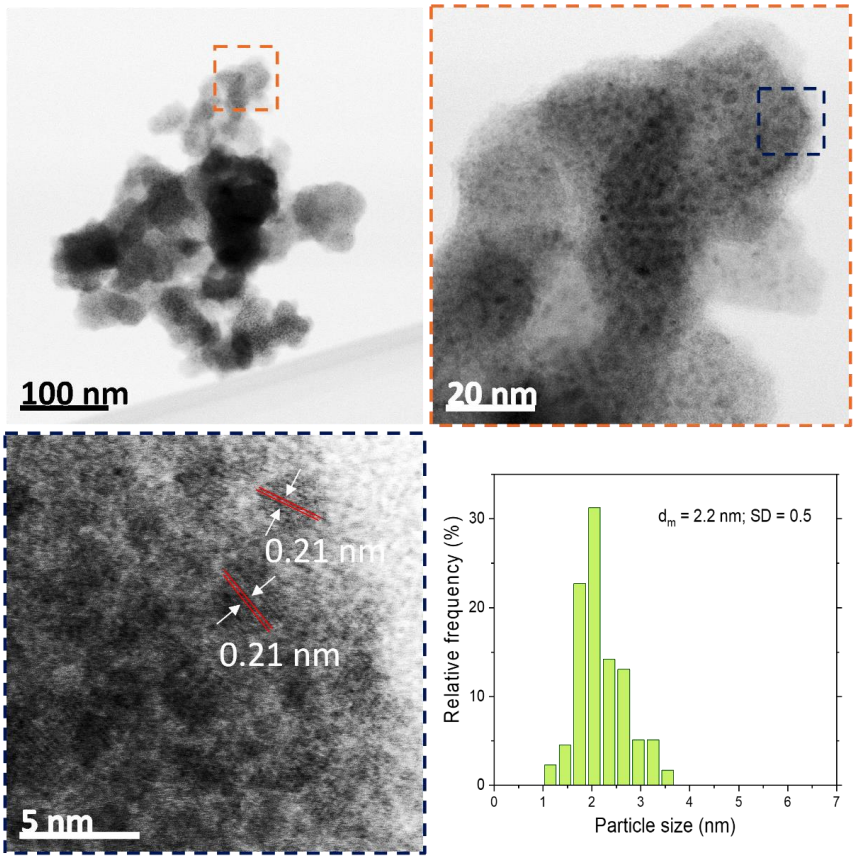

Figure 1. Representative TEM micrographs acquired at different magnifications and estimated particle size distribution of Ni/CTF^{Ph} (**1**).

Table 1. Ni loading, SSA and pore size distribution of Ni/CTF^{Ph} (**1**) and Ni/VXC (**2**).

Catalyst	Ni loading[a] [wt. %]	SSA[b] [$m^2\ g^{-1}$]	$V_{p(total)}$[c] [$cm^3\ g^{-1}$]	$V_{p(micro)}$[d] [$cm^3\ g^{-1}$]	$V_{p(micro)}$[d] [%]
Ni/CTF^{Ph} (**1**)	10.0	1923	1.36	0.47	34
Ni/VXC (**2**)	10.0	137	0.33	0.01	3

[a] Determined by ICP-OES. [b] Brunauer-Emmett-Teller (BET) specific surface area (SSA) measured by N_2 adsorption-desorption isotherms at 77 K. [c] Total pore volume determined using the adsorption branch of N_2 isotherm at p/p0 = 0.98. [d] Micropore volume calculated through NLDFT approximation.

To get further insight on materials chemical composition, **1** and **2** were further characterized by X-ray Photoelectron Spectroscopy (XPS). Survey spectra of both samples highlighted the expected elemental composition made of C, N, O and Ni and C, O and Ni for **1** and **2**, respectively (Figure S6). Notably, we did not reveal any appreciable contamination of Zn species on sample **1**, hence confirming the effectiveness of the adopted CTF^{Ph} workup procedure. High-resolution C 1*s* spectra of **1** and **2** (Figure S6) show a major signal at 284.6 eV due to C-C networks together with a minor component at 288.3 ± 0.2 eV ascribed to oxidized carbon species *(i.e.*, C-O groups). An additional component for **1**, located at 286.2 eV is finally ascribed to C-N functionalities.[54] The high-resolution N 1*s* XPS spectrum on Ni/CTF^{Ph} (**1**) (Figure 2C) presents a relatively large profile that can be fitted by five distinct components: those centered at 398.2 ± 0.2, 399.9 ± 0.2 and 401.1 ± 0.2 eV are respectively attributed to N-pyridinic, N-pyrrolic and N-graphitic sites of the amorphous CTF network as it results from the partial thermal decomposition/rearrangement of the original triazine-cores. A further component at 399.4 ± 0.2 eV is indicative of the interaction between the N-rich CTF support with the nickel active phase (Ni NPs) whereas the minor shoulder at higher BEs (402.0 ± 0.2 eV) is attributed to N-oxide species resulting from adventitious oxygen/moisture contaminations in the synthetic mixture.[55-57] Finally, the high-resolution Ni 2*p* XPS spectra recorded for both samples (Figure 2D) show the presence of two Ni $2p^{3/2}$ components for both

Ni/VXC (**2**) and Ni/CTF^{Ph} (**1**) (blue lines, Figure 2D) ascribed to generation of Ni^{2+}/Ni^{3+} species[58,59] by the spontaneous Ni(0) NPs oxidation upon their exposure to air during the material workup. The higher Ni 2*p* BE values registered for **1** respect to **2** is basically ascribed to electrostatic material charging during the analysis because of the semiconducting properties of CTF samples.[60,61] The additional two peaks observed at higher BE values (blue dotted lines on Figure 2D) were attributed to satellites.

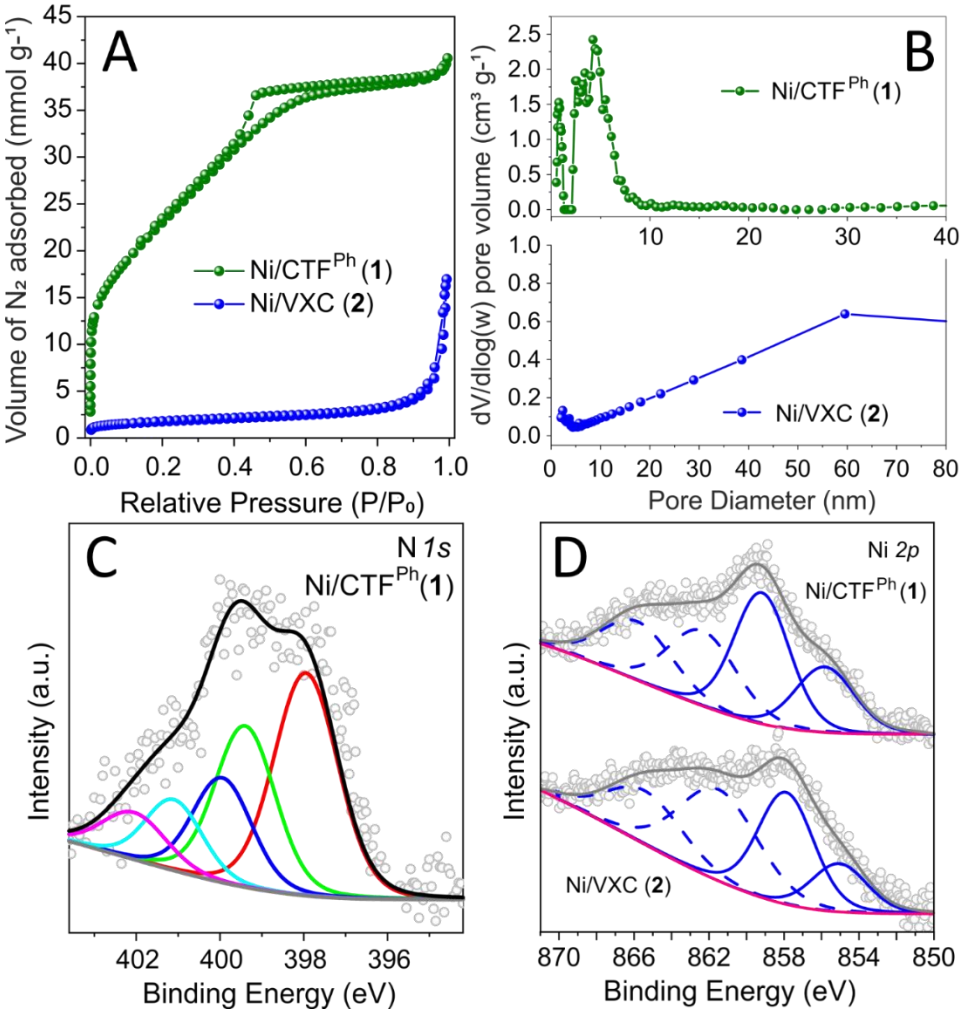

Figure 2. **A**) N_2 adsorption-desorption isotherms of Ni/CTF^{Ph} (**1**) (green curve) and Ni/VXC (**2**) (blue curve) registered at 77 K along with (**B**) their respective pore size distribution; **C**) high resolution N 1s core region of Ni/CTF^{Ph} (**1**) and (**D**) Ni 2p spectra of Ni/CTFPh (**1**) (upper part) and Ni/VXC (**2**) (lower part), dotted blue lines refer to satellite peaks.

3.2. Catalytic activity of Ni-catalysts in AB hydrolysis

Ni/CTF^{Ph} (**1**) was firstly tested for the hydrolytic dehydrogenation of AB under mild experimental conditions (*i.e.*, 30 °C) and its performance was compared with that of Ni/VXC (**2**) (Figure 3A). Both catalysts showed an induction time (t_i) (see Figure S7), that was ascribed to the reduction of the nickel oxides to Ni(0) by AB (see XPS and EELS analysis, Section 3.1). Afterwards, H_2 evolution started and grew up till reaching 3.0 equiv. of H_2 *per* mole of AB. As shown in Figure 3A, **2** required about 70 min to complete the AB hydrolysis thus resulting in a Turnover Frequency (TOF) of 3.3 min^{-1}. On the other hand, **1** showed a net superior performance in the process with a TOF over four times higher (TOF = 14.3 min^{-1}) than that of **2**. The activity gap measured between **1** and **2** has firstly been ascribed to the superior Ni NPs dispersion on CTF^{Ph} carrier featured by a higher SSA respect to VXC. In addition, the stronger metal-support interaction on the N-doped CTF^{Ph} is thought to favor a more effective electron transfer to the antibonding orbital of interacting H_2O molecules, though the intervening Ni NPs, which ultimately speed up the hydrogen evolution process.[23] For the sake of completeness, an additional catalytic trial was carried out using the plain CTF^{Ph} sample as catalyst. As outlined in Figure 3A (red curve), the bare support did not show any activity in the process hence implying the mandatory role of Ni NPs as the active components for the process to occur. Moreover, comparing results of **1** with those reported in the literature for AB hydrolysis (Table S1 and references cited therein), it is possible to conclude the central role played by the CTF^{Ph} support, combined with MVS to generate size-controlled Ni NPs, to provide one of the highest catalytic efficiency reported to date for monometallic nickel-based heterogeneous catalysts in the hydrolysis of AB. We have finally calculated the activation energy (E_a) of AB hydrolysis with both catalytic systems **1** and **2**. The rate of dihydrogen evolution in the presence of each catalyst was determined at three different

temperatures (30 °C, 45 °C and 60 °C), and then fitted with the Arrhenius equation (Figure S8). Accordingly, E_a values of 34.8 ± 3.6 kJ mol^{-1} and 32.1 ± 3.3 kJ mol^{-1}, consistent with previously reported data,[62,63] were calculated for Ni/CTF^{Ph} **1** and Ni/VXC **2**, respectively.

3.3. Catalytic activity of Ni-catalysts in the AB-TH to nitroaromatics

Ni/CTF^{Ph} (**1**) was then investigated as catalyst for the AB transfer hydrogenation (TH) to a variety of nitroaromatic compounds. To this aim, 4-nitrophenol hydrogenation was selected to optimize the AB TH conditions with **1** as catalyst in water at 30 °C. The process is an interesting solution to the conversion of toxic 4-nitrophenol present as pollutant in wastewater, into the more challenging 4-aminophenol.[64] As shown in Figure 3, Ni/CTF^{Ph} (**1**) promoted TH much more efficiently than the benchmark Ni/VXC catalyst (**2**). In fact, while **1** led to ca. 80 % selective conversion of 4-nitrophenol into 4-aminophenol in 180 minutes, (TOF = 5.3 h^{-1}), only 12% of conversion was observed in the same reaction time when **2** was used as the catalyst (TOF = 0.8 h^{-1}). Under these conditions, a complete conversion of 4-nitrophenol into 4-aminophenol was achieved using **1** as catalyst after 240 minutes. Besides the effects already discussed on the activation of AB, the superior catalytic activity of **1** in the 4-nitrophenol AB-TH can be tentatively ascribed to a more favorable adsorption/interaction of the phenolic substrate (and its intermediates) with the N-rich and highly basic support.[36,44,64]

Afterwards, **1** was investigated for the AB TH of a series of ortho- and para-substituted nitroaromatics (see Table 2). All runs were carried out at the optimized conditions (45 °C) used to get a quantitative conversion of 4-nitrophenol into 4-aminophenol (Entry 1, Table 2; the high efficiency and selectivity of the process was confirmed by ^{1}H NMR analysis of the crude reaction mixture – see Figure S9) but variable reaction times. The TH of 4-nitroaniline in pure water yielded the 4-phenylenediamine quantitatively after 10 minutes only (Entry 2, Table 2). To improve the

solubility of the less polar substrates, further TH trials (Entries 3-7, Table 2) were carried out in H_2O-EtOH (10:1).

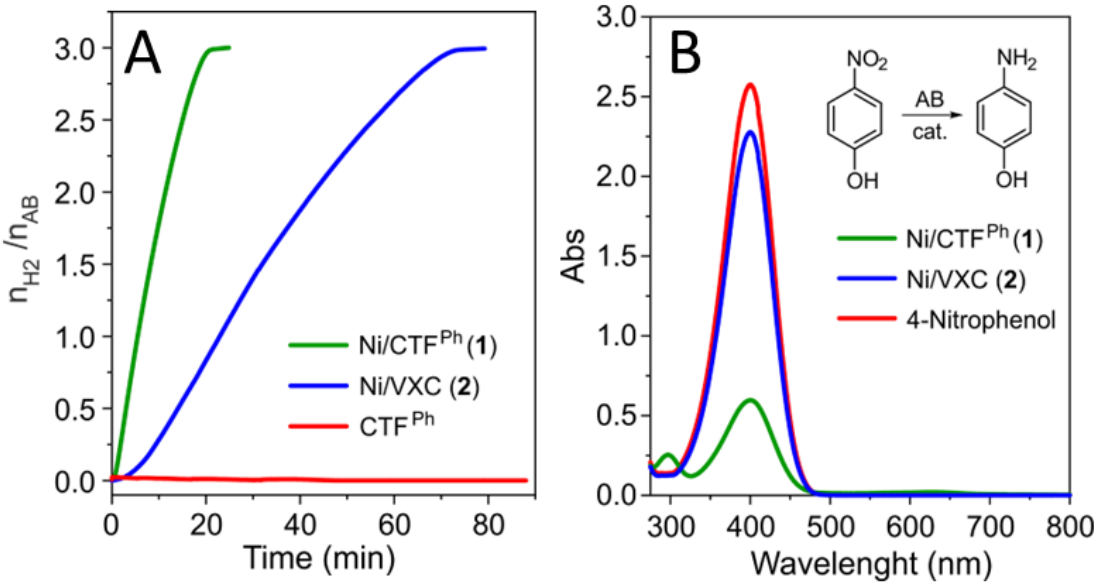

Figure 3. A) Moles of evolved H_2 normalized by mol of AB *vs.* time in AB hydrolysis catalyzed by Ni/CTF^{Ph} (**1**, green line), Ni/VXC (**2**, blue line) and CTF^{Ph} (red line) respectively; B) UV-vis spectrum of 4-nitrophenol solution before the reaction (red line) and registered at T= 30 °C after 180 minutes from the beginning of the TH catalyzed by Ni/CTF^{Ph} (**1**, green line), and Ni/VXC (**2**, blue line).

Under these conditions, nitrobenzene showed a complete conversion to aniline within only 5 minutes (Entry 3, Table 2) while 1-chloro-2-nitrobenzene and 1-chloro-4-nitrobenzene (Entries 4-5, Table 2) were converted chemoselectively to the respective chloroanilines within 10 min without any trace of dehalogenated by-products.[65] In the same conditions 1-bromo-4-nitrobenzene (Entry 6, Table 2) showed only 80% conversion after 30 min, albeit with complete selectivity towards 4-bromoaniline. When catalysis with this substrate was carried out till its complete conversion (1 h), the selectivity to 4-bromoaniline decreased to 93% due to the formation of 7% aniline from C-Br cleavage.

Table 2. Ni/CTF^{Ph} (**1**) promoted TH reactions of nitroaromatic compounds.

Entry	Substrate	Main product	Time [min]	Conversion [%]	Selectivity [%]
1	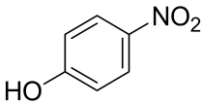	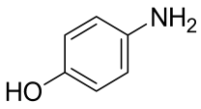	40	>99.9[b]	>99.9
2[a]	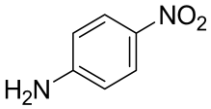	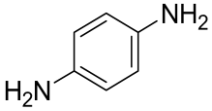	10	>99.9[b]	>99.9
3[c]	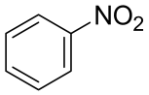	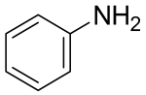	5	>99.9[d]	>99.9
4[c]	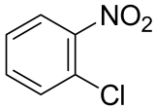	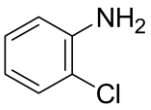	10	>99.9[d]	99.9
5[c]	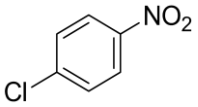	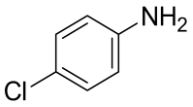	10	>99.9[d]	>99.9
6[c,f]	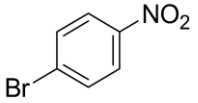	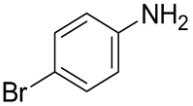	60	>99.9[d]	93.0
7[e]	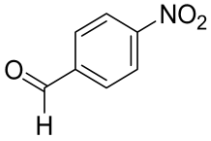	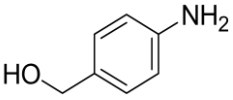	110	>99.9[d]	>99.9

[a] Reaction condition: 0.052 mmol nitroarene, 0.0026 mmol Ni, 0.25 mmol AB, 3 mL of H_2O, 45 °C. [b] Conversion was determined by UV-VIS. [c] Reaction condition: 0.130 mmol nitroarene, 0.0026 mmol Ni, 0.25 mmol AB, 3 mL of H_2O-EtOH (10:1), 45 °C. [d] Conversion and selectivity were determined by GC-FID. [e] Reaction condition: 0.130 mmol nitroarene, 0.0026 mmol Ni, 0.65 mmol AB, 3 mL of H_2O-EtOH (10:1), 45 °C. [f] The crude contained 7% aniline by-product by GC-MS.

According to the literature, the higher propensity of 1-bromo-4-nitrobenzene to give the dehalogenated by-product with respect to 1-chloro-4-nitrobenzene may be related to the different strength of carbon-halogen bonds (340.2 kJ/mol and 281.4 kJ/mol for C–Cl and C–Br, respectively).[66] Interestingly, in the case of 4- nitrobenzaldehyde, the carbonyl group was reduced by AB to the corresponding benzyl alcohol (> 99.9 % selectivity), even in the absence of any

catalyst.[67] However, to get TH of nitro group (Entry 7, Table 2) Ni/CTF^{Ph} (**1**) catalyst was needed along with 5 equiv. of AB with respect to the substrate. Under these conditions, the total conversion of the starting material to 4-aminobenzyl alcohol was obtained in about 110 min. This substrates screening highlights the versatility of the Ni/CTF^{Ph} system with respect to AB TH under mild experimental conditions.

ICP-OES analysis of the reaction mixture of 4-nitrophenol TH (Entry 1, Table 2) after catalyst removal showed a very low Ni-leaching in solution, less than 2.5 wt.% of the metal amount in pristine **1**. This result prompted the examination of catalyst recycling in batch, which was studied by taking the AB TH of 4-nitrophenol as the benchmark reaction. With this goal, the solid catalyst recovered at the end of the first catalytic run (entry 1, Table 2) was washed and recycled under identical experimental conditions (see section 2.5 for details); this recovering/recycling test was operated for six successive runs. As summarized in Figure 4, **1** (always at the fixed reaction time: 40 min.) maintained its performance almost unchanged during the second catalytic cycle showing an almost complete conversion of 4-nitrophenol (98 %) with a selectivity > 99.9%. During the next catalytic cycles, a slight conversion decrease was measured till the last recycling test (sixth) where it dropped down to 86 %. This moderate conversion decrease was ascribed to an unavoidable loss of the catalytic material during the transfer and washing steps between one cycle and the next one.

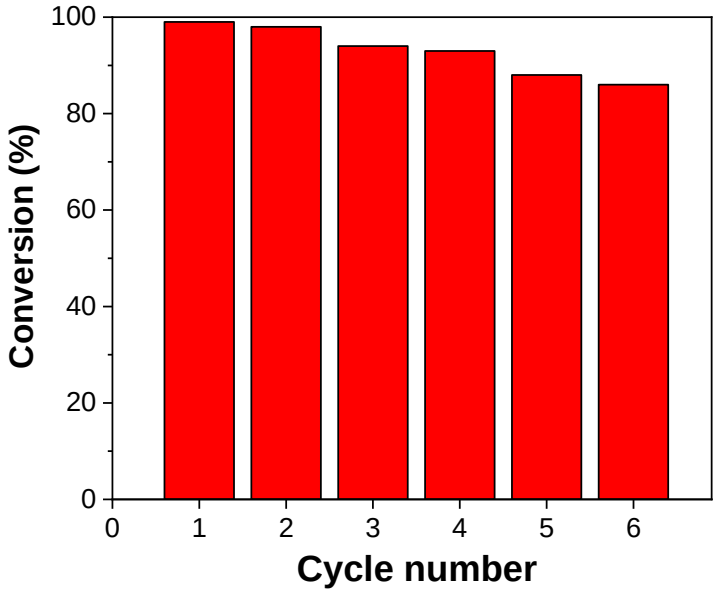

Figure 4. Conversion of 4-nitrophenol over Ni/CTF^{Ph} (**1**) over 6 reaction cycles. Reaction conditions: Ni/CTF^{Ph} (**1**) 10.0 wt. Ni% (6 mg, 0.0102 mmol Ni), 4-nitrophenol (0.21 mmol), AB (1.0 mmol), T = 45 °C, t = 40 min. P_n = 115 $mol_{product}$ mol_{Ni}^{-1}.

Representative TEM micrographs (see Figure S10) have confirmed the stability of the six-times reused catalyst that exhibited a virtually unchanged size and distribution of Ni NPs with respect to its freshly prepared counterpart.

To get more details on the reaction mechanism at work in the hydrogenation process catalyzed by **1** (hydrogenation *vs*. hydrogen transfer), selected experiments under specific conditions have been carried out (see Figure S11). In particular, the quantitative nitrobenzene reduction to aniline (Table 2, entry 3) was obtained in 5 minutes regardless the use of an open or closed reaction vessel. This result suggests that the process kinetic was negligibly affected by the H_2 concentration in the reaction medium. In addition, when the reaction was carried out bubbling gaseous H_2 in the place of $H_3N{\cdot}BH_3$ as hydrogen source or TH reagent, no substrate conversion was detected to any extent. According to these (indirect) experiments and previously reported data for related systems [3], this

result unambiguously indicates that molecular H_2 deriving from AB dehydrogenation was not directly involved in the process.

As an additional proof of the catalyst stability on run, the **1** mediated AB TH to 4-nitrophenol was tested in a continuous flow setup (Figure S12). To this aim, pre-heated (45 °C) water solutions of AB and 4-nitrophenol (0.5 M and 0.017 M, respectively) were mixed in 5:1 molar ratio with the aid of a FlowLab^{TM} pumping system and passed at the same temperature through a stainless steel reactor containing **1** (for a schematic representation of the device, see Figure S12). Despite the total flow-rate adopted in the experiment (f_{A+B} = 0.48 mL min^{-1}) led to a residence time of the reactants in the catalytic section of 5.2 min only, complete conversion of 4-nitrophenol was recorded at the reactor outlet in the course of three consecutive runs lasting 2 h each (6 h total time on stream, TTOS). Interestingly, despite the cumulative productivity (P_n, $mol_{product}\, mol_{Ni}^{-1}$) at the end of the continuous flow run (P_n = 61) was comparable to that attained in the first three batch cycles described above, no appreciable loss of catalytic activity was observed for the entire duration of the experiment (Figure S13). Moreover, ICP-OES analysis of the solution collected at the outlet of the continuous flow reactor showed that Ni leaching (1 wt.% of the initial total Ni amount) was lower that in the batch. Together with the prevention of the mechanical losses of catalytic material suffered on going to a batch run to the next one, this fact could explain the better stability of **1** in the continuous flow system and confirming its promising robustness and durability under AB TH conditions.

Overall, the catalytic procedure for the selective reduction of nitroarenes to anilines, described herein, possess some distinctive advantages over the other literature examples that make use of Ni-based systems (Table S2 and references therein). Particularly, the AB TH in the presence of Ni/CTF^{Ph} appears to proceed under much milder reaction conditions (P = 0.1 MPa, 45 °C) than

with the published procedures involving H_2 as the reducing agent (P = 1.5 – 3 MPa, T = 100 – 210 °C). Moreover, for most of the substrates examined herein (see Table 2) the attainment of complete conversion turned out to be a matter of minutes, instead of hours (0.5-12 h) as in the TH examples reported to date in the literature (which, as summarized in Table S2, made use of reducing agents different from AB: hydrazine hydrate, $NaBH_4$, formic acid or isopropanol).

4. CONCLUSIONS

To summarize, the combination of a non-innocent CTF^{Ph} carrier with the MVS approach has allowed to generate a nanocomposite featured by ultrasmall and highly dispersed Ni NPs (mean diameter 2.2 nm). The catalyst has successfully been employed to promote AB hydrolysis for H_2 evolution and the selective AB-TH with a series of variably substituted nitroarenes, including challenging haloarenes, to give the corresponding anilines under exceptionally mild experimental conditions (*i.e.,* near atmospheric pressure, 45 °C, 5-110 min). Ni/CTF^{Ph} has shown superior performance on both processes with respect to a MVS-derived system prepared on a plain C-support as well as related Ni-based heterogeneous systems of the *state-of-the-art*. Particularly, in the AB-TH of 2- and 4-chloronitrobenzene a complete selectivity towards the corresponding chloroanilines was achieved. The catalyst efficiency, stability and durability on long-term catalytic runs have been confirmed under batch through successive recovery/washing and re-use of the catalytic material and in a continuous flow reactor setup. All in all, the nanocomposite described in the contribution candidates to replace less sustainable and more expensive catalysts (*i.e.*, those deriving from PGMs) for the AB hydrolysis and AB-TH of nitroarenes under exceptionally mild experimental conditions.

AUTHOR INFORMATION

Corresponding Authors:

*Claudio Evangelisti: claudio.evangelisti@cnr.it

*Giuliano Giambastiani: giuliano.giambastiani@iccom.cnr.it

Author Contributions

The manuscript was written through contributions of all authors. All authors have given approval to the final version of the manuscript. CRediT: **Esther Punzi**: formal analysis, investigation, writing-review & editing; **Xuan Trung Nguyen**: data curation, writing-review & editing; **Emanuela Pitzalis**: data curation, formal analysis, writing-review & editing; **Alessandro Mandoli**: data curation, formal analysis, writing-review & editing; **Massimo Onor**: formal analysis; **Lorenzo Poggini**: formal analysis; **Giulia Tuci**: data curation, formal analysis, writing-review & editing; **Giuliano Giambastiani**: conceptualization, data curation, formal analysis, writing-review & editing; **Claudio Evangelisti**: conceptualization, formal analysis, funding acquisition, methodology, project administration, supervision, writing-review & editing.

Funding Sources

This research was funded by the European Union – NextGeneration EU through the Italian Ministry of Environment and Energy Security POR H2 AdP MMES/ENEA with involvement of CNR and RSE, PNRR - Mission 2, Component 2, Investment 3.5 “Ricerca e sviluppo sull’idrogeno”, CUP: B93C22000630006. E. P. and C. E. would like to thank the Italian MUR through the PRIN2022 project “MAGICAT- MAGnetic Inductive heating of nano-CATalyst onto metal foam as innovative approach for selective aerobic alcohol and polyol oxidation”

(20225RBM98). G. G. and G. T. would like to thank the Italian MUR through the PRIN2022 project “MATISSE - A "Molecular Lift" for the Control of the Metal Protrusion and Coordination Sphere in Single-Atom Catalysts for CO_2 Electroreduction” (2022K5SX27).

SUPPORTING INFORMATION

Representative scheme of experimental setups; Additional characterization by transmission electron microscopy and XPS techniques, additional XP; 1H-NMR spectra; Comparative analysis of the state-of-the-art.

ACKNOWLEDGMENT

The authors thank Mr. Brunetto Cortigiani for his assistance in using the MatchLab platform.

ABBREVIATIONS

AB, Ammonia borane; BE, Binding energy; BET, Brunauer-Emmet-Teller; CTF, Covalent Triazine Frameworks; E_a, Activation energy; GC-FID, Gas chromatography-flame ionization detector; GC-MS, Gas chromatography-mass spectrometry; ICP-OES, Inductively coupled plasma-optical emission spectrometers; MVS, Metal vapor synthesis; NLDFT, Non-local density function theory; NPs, Nanoparticles; P_n, Productivity; PCFR, Packed-bed continuous-flow reactor; SMA, Solvated metal atom; SSA, Specific surface area; TEM, Trasmission electron microscopy; TH, Transfer hydrogenation; TOF, Turnover Frequency; TTOS, total time on stream; VXC, Carbon Vulcan XC-72R; XPS, X-ray photoelectron spectroscopy.

REFERENCES

(1) Akbayrak, S.; Özkar, S. Ammonia Borane as Hydrogen Storage Materials. *Int. J. Hydrogen Energy* **2018**, *43* (40), 18592–18606.

(2) Usman, M. R. Hydrogen Storage Methods: Review and Current Status. *Renew. Sust. Energy Rev*. **2022**, 112743.

(3) Zhao, W.; Li, H.; Zhang, H.; Yang, S.; Riisager, A. Ammonia Borane-Enabled Hydrogen Transfer Processes: Insights into Catalytic Strategies and Mechanisms. *Green Energy and Environment.* **2022**.

(4) Alonso, F.; Riente, P.; Yus, M. Nickel Nanoparticles in Hydrogen Transfer Reactions. *Acc. Chem. Res.* **2011**, *44* (5), 379–391.

(5) Nie, R.; Tao, Y.; Nie, Y.; Lu, T.; Wang, J.; Zhang, Y.; Lu, X.; Xu, C. C. Recent Advances in Catalytic Transfer Hydrogenation with Formic Acid over Heterogeneous Transition Metal Catalysts. *ACS Catal.* **2021**, *11* (3), 1071–1095.

(6) Haoran, W.; Lingyi, L.; Biao, X.; Yong, L.; Xiaobao, Z.; Xiaodong, Q. Nickel-Catalyzed Transfer Hydrogenation of Unactivated Aryl Alkenes with Hydrosilane as Hydrogen Source. *Asian. J. Org. Chem.* **2023**, *12* (1), e202200590.

(7) Lau, S.; Gasperini, D.; Webster, R. L. Amine–Boranes as Transfer Hydrogenation and Hydrogenation Reagents: A Mechanistic Perspective. *Angew. Chem. Int.* **2021**, *60* (26), 14272–14294.

(8) Shabir, J.; Garkoti, C.; Gupta, P.; Sharma, M.; Rani, S.; Kumari, M.; Mozumdar, S. RuxPdyAlloy Nanoparticles Uniformly Anchored on Reduced Graphene Oxide Nanosheets (RuxPdy@rGO): A Recyclable Catalyst. *ACS Omega* **2021**, *6* (2), 1415–1425.

(9) Yan, J. M.; Zhang, X. B.; Akita, T.; Haruta, M.; Xu, Q. One-Step Seeding Growth of Magnetically Recyclable AU@Co Core-Shell Nanoparticles: Highly Efficient Catalyst for Hydrolytic Dehydrogenation of Ammonia Borane. *J. Am. Chem. Soc.* **2010**, *132* (15), 5326–5327.

(10) Chandra, M.; Xu, Q. Room Temperature Hydrogen Generation from Aqueous Ammonia-Borane Using Noble Metal Nano-Clusters as Highly Active Catalysts. *J. Power Sources* **2007**, *168* (1 SPEC. ISS.), 135–142.

(11) Muzzio, M.; Lin, H.; Wei, K.; Guo, X.; Yu, C.; Yom, T.; Xi, Z.; Yin, Z.; Sun, S. Efficient Hydrogen Generation from Ammonia Borane and Tandem Hydrogenation or Hydrodehalogenation over AuPd Nanoparticles. *ACS Sustain. Chem. Eng.* **2020**, *8* (7), 2814–2821.

(12) Byun, S.; Song, Y.; Kim, B. M. Heterogenized Bimetallic Pd-Pt-Fe3O4 Nanoflakes as Extremely Robust, Magnetically Recyclable Catalysts for Chemoselective Nitroarene Reduction. *ACS Appl. Mater. Interfaces* **2016**, *8* (23), 14637–14647.

(13) Song, Q.; Wang, W. D.; Hu, X.; Dong, Z. Ru Nanoclusters Confined in Porous Organic Cages for Catalytic Hydrolysis of Ammonia Borane and Tandem Hydrogenation Reaction. *Nanoscale* **2019**, *11* (44), 21513–21521.

(14) Du, J.; Chen, J.; Xia, H.; Zhao, Y.; Wang, F.; Liu, H.; Zhou, W.; Wang, B. Commercially Available CuO Catalyzed Hydrogenation of Nitroarenes Using Ammonia Borane as a Hydrogen Source. *ChemCatChem* **2020**, *12* (9), 2426–2430.

(15) Li, P.; Chen, R.; Zhao, S.; Li, W.; Lin, Y.; Yu, Y. Architecture Control and Electronic Structure Engineering over Ni-Based Nitride Nanocomposite for Boosting Ammonia Borane Dehydrogenation. *Appl. Catal. B* **2021**, *298*.

(16) Zhou, Y. H.; Wang, S.; Wan, Y.; Liang, J.; Chen, Y.; Luo, S.; Yong, C. Low-Cost CuNi-CeO2/RGO as an Efficient Catalyst for Hydrolysis of Ammonia Borane and Tandem Reduction of 4-Nitrophenol. *J. Alloys Compd.* **2017**, *728*, 902–909.

(17) Shen, M.; Liu, H.; Yu, C.; Yin, Z.; Muzzio, M.; Li, J.; Xi, Z.; Yu, Y.; Sun, S. Room-Temperature Chemoselective Reduction of 3-Nitrostyrene to 3-Vinylaniline by Ammonia Borane over Cu Nanoparticles. *J. Am. Chem. Soc.* **2018**, *140* (48), 16460–16463.

(18) Yu, C.; Fu, J.; Muzzio, M.; Shen, T.; Su, D.; Zhu, J.; Sun, S. CuNi Nanoparticles Assembled on Graphene for Catalytic Methanolysis of Ammonia Borane and Hydrogenation of Nitro/Nitrile Compounds. *Chem. Mat.* **2017**, *29* (3), 1413–1418.

(19) Zhou, L.; Meng, J.; Li, P.; Tao, Z.; Mai, L.; Chen, J. Ultrasmall Cobalt Nanoparticles Supported on Nitrogen-Doped Porous Carbon Nanowires for Hydrogen Evolution from Ammonia Borane. *Mater. Horiz.* **2017**, *4* (2), 268–273.

(20) Zahmakiran, M.; Özkar, S. Transition Metal Nanoparticles in Catalysis for the Hydrogen Generation from the Hydrolysis of Ammonia-Borane. *Top. Catal.* **2013**, *56* (13–14), 1171–1183.

(21) Umegaki, T.; Yan, J. M.; Zhang, X. B.; Shioyama, H.; Kuriyama, N.; Xu, Q. Preparation and Catalysis of Poly(N-Vinyl-2-Pyrrolidone) (PVP) Stabilized Nickel Catalyst for Hydrolytic Dehydrogenation of Ammonia Borane. *Int. J. Hydrogen Energy* **2009**, *34* (9), 3816–3822.

(22) Yan, J. M.; Zhang, X. B.; Han, S.; Shioyama, H.; Xu, Q. Iron-Nanoparticle-Catalyzed Hydrolytic Dehydrogenation of Ammonia Borane for Chemical Hydrogen Storage. *Angew. Chem. Int.* **2008**, *47* (12), 2287–2289.

(23) Li, Z.; He, T.; Liu, L.; Chen, W.; Zhang, M.; Wu, G.; Chen, P. Covalent Triazine Framework Supported Non-Noble Metal Nanoparticles with Superior Activity for Catalytic Hydrolysis of Ammonia Borane: From Mechanistic Study to Catalyst Design. *Chem. Sci.* **2016**, *8* (1), 781–788.

(24) Metin, Ö.; Mazumder, V.; Özkar, S.; Sun, S. Monodisperse Nickel Nanoparticles and Their Catalysis in Hydrolytic Dehydrogenation of Ammonia Borane. *J. Am. Chem. Soc*. **2010**, *132* (5), 1468–1469.

(25) Lin, Y.; Yang, L.; Jiang, H.; Zhang, Y.; Cao, D.; Wu, C.; Zhang, G.; Jiang, J.; Song, L. Boosted Reactivity of Ammonia Borane Dehydrogenation over Ni/Ni 2 P Heterostructure. *J. Phys. Chem. Lett.* **2019**, *10* (5), 1048–1054.

(26) Wang, C.; Tuninetti, J.; Wang, Z.; Zhang, C.; Ciganda, R.; Salmon, L.; Moya, S.; Ruiz, J.; Astruc, D. Hydrolysis of Ammonia-Borane over Ni/ZIF-8 Nanocatalyst: High Efficiency, Mechanism and Controlled Hydrogen Release. *J. Am. Chem. Soc.* **2017**, *139* (33), 11610-11615.

(27) Pagliaro, M. V.; Miller, H. A.; Evangelisti, C.; Bellini, M.; Tuci, G.; Pham-Huu, C.; Giambastiani, G.; Marelli, M.; Vizza, F. Synergy between Nickel Nanoparticles and N-Enriched Carbon Nanotubes Enhances Alkaline Hydrogen Oxidation and Evolution Activity. *ACS Appl. Nano. Mater.* **2021**, *4* (4), 3586–3596.

(28) Qin, Q.; Chen, L.; Wei, T.; Wang, Y.; Liu, X. Ni/NiM2O4 (M = Mn or Fe) Supported on N-Doped Carbon Nanotubes as Trifunctional Electrocatalysts for ORR, OER and HER. *Catal.. Sci. Technol.* **2019**, *9* (7), 1595–1601.

(29) Zhuang, Z.; Giles, S. A.; Zheng, J.; Jenness, G. R.; Caratzoulas, S.; Vlachos, D. G.; Yan, Y. Nickel Supported on Nitrogen-Doped Carbon Nanotubes as Hydrogen Oxidation Reaction Catalyst in Alkaline Electrolyte. *Nat. Commun*. **2016**, *7* (1), 10141.

(30) Wang, W.; Duong-Viet, C.; Ba, H.; Baaziz, W.; Tuci, G.; Caporali, S.; Nguyen-Dinh, L.; Ersen, O.; Giambastiani, G.; Pham-Huu, C.; Vien, P.; Thang, D.; Tu Liem, B. Nickel Nanoparticles Decorated Nitrogen-Doped Carbon Nanotubes (Ni/ N-CNT); a Robust Catalyst for the Efficient and Selective CO 2 Methanation. *ACS. Appl. Energy Mater.* **2018**, *2* (2), 1111-1120.

(31) Katekomol, P.; Roeser, J.; Bojdys, M.; Weber, J.; Thomas, A. Covalent Triazine Frameworks Prepared from 1,3,5-Tricyanobenzene. *Chem. Mat.* **2013**, *25* (9), 1542–1548.

(32) Liu, M.; Guo, L.; Jin, S.; Tan, B. Covalent Triazine Frameworks: Synthesis and Applications. *J. Mat. Chem. A* **2019**, *7* (10), 5153–5172.

(33) Krishnaraj, C.; Jena, H. S.; Leus, K.; Van Der Voort, P. Covalent Triazine Frameworks-a Sustainable Perspective. *Green Chem.* **2020**, *22* (4), 1038–1071.

(34) Liao, L.; Li, M.; Yin, Y.; Chen, J.; Zhong, Q.; Du, R.; Liu, S.; He, Y.; Fu, W.; Zeng, F. Advances in the Synthesis of Covalent Triazine Frameworks. *ACS Omega* **2023**, *8* (5), 4527–4542.

(35) Puthiaraj, P.; Lee, Y. R.; Zhang, S.; Ahn, W. S. Triazine-Based Covalent Organic Polymers: Design, Synthesis and Applications in Heterogeneous Catalysis. *J. Mater. Chem. A* **2016**, *4* (42), 16288–16311.

(36) Tuci, G.; Pilaski, M.; Ba, H.; Rossin, A.; Luconi, L.; Caporali, S.; Pham-Huu, C.; Palkovits, R.; Giambastiani, G. Unraveling Surface Basicity and Bulk Morphology Relationship on Covalent Triazine Frameworks with Unique Catalytic and Gas Adsorption Properties. *Adv. Funct. Mater.* **2017**, *27* (7), 1605672.

(37) Iemhoff, A.; Deischter, J.; Jung, S.; Tuci, G.; Giambastiani, G.; Palkovits, R. Polymer-Inspired Covalent Triazine Frameworks from the Carbonaceous Side - Influence of Unexpected Surface Functionalisation on Liquid-Phase Adsorption Processes. *J. Mater. Chem. A* **2021**, *9* (9), 5390–5403.

(38) Yu, W.; Gu, S.; Fu, Y.; Xiong, S.; Pan, C.; Liu, Y.; Yu, G. Carbazole-Decorated Covalent Triazine Frameworks: Novel Nonmetal Catalysts for Carbon Dioxide Fixation and Oxygen Reduction Reaction. *J. Catal.* **2018**, *362*, 1–9.

(39) Hug, S.; Stegbauer, L.; Oh, H.; Hirscher, M.; Lotsch, B. V. Nitrogen-Rich Covalent Triazine Frameworks as High-Performance Platforms for Selective Carbon Capture and Storage. *Chem. Mat.* **2015**, *27* (23), 8001–8010.

(40) Li, Y.; Zheng, S.; Liu, X.; Li, P.; Sun, L.; Yang, R.; Wang, S.; Wu, Z. S.; Bao, X.; Deng, W. Q. Conductive Microporous Covalent Triazine-Based Framework for High-Performance Electrochemical Capacitive Energy Storage. *Angew. Chem. Int.* **2018**, *57* (27), 7992–7996.

(41) Guo, L.; Niu, Y.; Xu, H.; Li, Q.; Razzaque, S.; Huang, Q.; Jin, S.; Tan, B. Engineering Heteroatoms with Atomic Precision in Donor-Acceptor Covalent Triazine Frameworks to Boost Photocatalytic Hydrogen Production. *J. Mater. Chem. A* **2018**, *6* (40), 19775–19781.

(42) Zhu, G.; Shi, S.; Liu, M.; Zhao, L.; Wang, M.; Zheng, X.; Gao, J.; Xu, J. Formation of Strong Basicity on Covalent Triazine Frameworks as Catalysts for the Oxidation of Methylene Compounds. *ACS Appl. Mater. Interfaces* **2018**, *10* (15), 12612–12617.

(43) Li, Z.; He, T.; Matsumura, D.; Miao, S.; Wu, A.; Liu, L.; Wu, G.; Chen, P. Atomically Dispersed Pt on the Surface of Ni Particles: Synthesis and Catalytic Function in Hydrogen Generation from Aqueous Ammonia-Borane. *ACS Catal.* **2017**, *7* (10), 6762–6769.

(44) Wang, J.; Yu, Y.; Xu, W.; Yu, H.; Zhang, W.; Huang, H.; Zhang, G. R.; Mei, D. Covalent Triazine Framework Encapsulated Pd Nanoclusters for Efficient Hydrogen Production via Ammonia Borane Hydrolysis. *J. Catal.* **2022**, *411,* 72–83.

(45) Pitzalis, E.; Psaro, R.; Evangelisti, C. From Metal Vapor to Supported Single Atoms, Clusters and Nanoparticles: Recent Advances to Heterogeneous Catalysts. *Inorganica Chim. Acta* **2022**, *533,* 120782.

(46) Jumde, R. P.; Evangelisti, C.; Mandoli, A.; Scotti, N.; Psaro, R. Aminopropyl-Silica-Supported Cu Nanoparticles: An Efficient Catalyst for Continuous-Flow Huisgen Azide-Alkyne Cycloaddition (CuAAC). *J. Catal*. **2015**, *324*, 25–31.

(47) Fusini, G.; Rizzo, F.; Angelici, G.; Pitzalis, E.; Evangelisti, C.; Carpita, A. Polyvinylpyridine-Supported Palladium Nanoparticles: An Efficient Catalyst for Suzuki–Miyaura Coupling Reactions. *Catalysts* **2020**, *10* (3), 330.

(48) Oberhauser, W.; Evangelisti, C.; Jumde, R. P.; Psaro, R.; Vizza, F.; Bevilacqua, M.; Filippi, J.; Machado, B. F.; Serp, P. Platinum on Carbonaceous Supports for Glycerol Hydrogenolysis: Support Effect. *J. Catal.* **2015**, *325*, 111–117.

(49) Campisi, S.; Palliggiano, S.; Gervasini, A.; Evangelisti, C. Finely Iron-Dispersed Particles on β Zeolite from Solvated Iron Atoms: Promising Catalysts for NH3-SCO. *J. Phys. Chem. C* **2019**, *123* (18), 11723–11733.

(50) Feng, L.; Ali, S.; Xu, C.; Cao, S.; Tuci, G.; Giambastiani, G.; Pham-Huu, C.; Liu, Y. Assessing the Nature of Active Sites on Nanodiamonds as Metal-Free Catalysts for the EB-to-ST Direct Dehydrogenation Using a Catalytic Approach. *ACS Catal.* **2022**, *12* (10), 6119–6131.

(51) Artz, J.; Mallmann, S.; Palkovits, R. Selective Aerobic Oxidation of Hmf to 2,5-Diformylfuran on Covalent Triazine Frameworks-Supported Ru Catalysts. *ChemSusChem* **2015**, *8* (4), 772–789.

(52) Holade, Y.; Morais, C.; Servat, K.; Napporn, T. W.; Kokoh, K. B. Enhancing the Available Specific Surface Area of Carbon Supports to Boost the Electroactivity of Nanostructured Pt Catalysts. *Phys. Chem. Chem. Phys.* **2014**, *16* (46), 25609–25620.

(53) Krishnankutty, N.; Albert Vannice, M. Effect of Pretreatment on Surface Area, Porosity, and Adsorption Properties of a Carbon Black. *Chem. Mater.* **1995**, *7* (4), 754-763.

(54) Xiong, Y.; Qin, Y.; Su, L.; Ye, F. Bioinspired Synthesis of Cu2+-Modified Covalent Triazine Framework: A New Highly Efficient and Promising Peroxidase Mimic. *Chem. Eur. J.* **2017**, *23* (46), 11037–11045.

(55) Osadchii, D. Y.; Olivos-Suarez, A. I.; Bavykina, A. V.; Gascon, J. Revisiting Nitrogen Species in Covalent Triazine Frameworks. *Langmuir* **2017**, *33* (50), 14278–14285.

(56) Tuci, G.; Iemhoff, A.; Rossin, A.; Yakhvarov, D.; Gatto, M. F.; Balderas-Xicohténcatl, R.; Zhang, L.; Hirscher, M.; Palkovits, R.; Pham-Huu, C.; Giambastiani, G. Tailoring Morphological and Chemical Properties of Covalent Triazine Frameworks for Dual CO2 and H2 Adsorption. *Int. J. Hydrogen Energy* **2022**, *47* (13), 8434–8445.

(57) Öztürk, S.; Xiao, Y. X.; Dietrich, D.; Giesen, B.; Barthel, J.; Ying, J.; Yang, X. Y.; Janiak, C. Nickel Nanoparticles Supported on a Covalent Triazine Framework as Electrocatalyst for Oxygen Evolution Reaction and Oxygen Reduction Reactions. *Beilstein J. Nanotechnol.* **2020**, *11*, 770–781.

(58) Chen, Q.; Yu, Y.; Zhou, S.; Sha, L.; Zhuang, G.; Wang, P.; Han, X. Electrocatalytic Overall Water Splitting Induced by Surface Reconstruction of an Iron-Modified Ni2P/Ni5P4 Heterojunction Array Encapsulated into a N-Doped Carbon Layer. *Inorg. Chem.* **2023**, *62* (16), 6518–6526.

(59) Wang, X.; Hu, J.; Su, Y.; Hao, J.; Liu, F.; Han, S.; An, J.; Lian, J. Ni Foam-Ni3S2@Ni(OH)2-Graphene Sandwich Structure Electrode Materials: Facile Synthesis and High Supercapacitor Performance. *Chem.-Eur. J.* **2017**, *23* (17), 4128–4136.

(60) Grosvenor, A. P.; Biesinger, M. C.; Smart, R. S. C.; McIntyre, N. S. New Interpretations of XPS Spectra of Nickel Metal and Oxides. *Surf. Sci.* **2006**, *600* (9), 1771–1779.

(61) Shestakov, M. S.; Vul, S. P.; Dideikin, A. T.; Larionova, T. V.; Shvidchenko, A. V.; Yudina, E. B.; Shnitov, V. V. Advanced Oxidation Process for Detonation Nanodiamond Surface Chemical Modification. *J. Phys. Conf. Ser.* **2019**, *1400* (5).

(62) Metin, Ö.; Özkar, S. Water Soluble Nickel(0) and Cobalt(0) Nanoclusters Stabilized by Poly(4-Styrenesulfonic Acid-Co-Maleic Acid): Highly Active, Durable and Cost Effective

Catalysts in Hydrogen Generation from the Hydrolysis of Ammonia Borane. *Int. J. Hydrogen Energy* **2011**, *36* (2), 1424–1432.

(63) Zhou, L.; Zhang, T.; Tao, Z.; Chen, J. Ni Nanoparticles Supported on Carbon as Efficient Catalysts for the Hydrolysis of Ammonia Borane. *Nano. Res.* **2014**, *7* (5), 774–781.

(64) Tian, X.; Zahid, M.; Li, J.; Sun, W.; Niu, X.; Zhu, Y. Pd/Mo2N-TiO2 as Efficient Catalysts for Promoted Selective Hydrogenation of 4-Nitrophenol: A Green Bio-Reducing Preparation Method. *J. Catal.* **2020**, *391*, 190–201.

(65) Wang, X.; Liang, M.; Zhang, J.; Wang, Y. Selective Hydrogenation of Aromatic Chloronitro Compounds. *Curr. Org. Chem.* **2007**, *11* (3), 299-314.

(66) Wu, W.; Xu, J.; Ohnishi, R. Complete Hydrodechlorination of Chlorobenzene and Its Derivatives over Supported Nickel Catalysts under Liquid Phase Conditions. *Appl. Catal. B* **2005**, *60* (1–2), 129–137.

(67) Faverio, C.; Boselli, M. F.; Medici, F.; Benaglia, M. Ammonia Borane as a Reducing Agent in Organic Synthesis. *Org. Biomol. Chem.* **2020**, *18* (39), 7789–7813.

TOC Graphic